



CIVIL 443
Advanced composites in engineering structures

Project

**Composite Laminate Optimization
for Prosthetic Feet**

Mehmet Furkan Doğan¹,
Ali Fuat Şahin¹,
Wissam Lasfar¹, and
Ulysse Adam Louis Closet¹

¹Section of Mechanical Engineering, École Polytechnique Fédérale de Lausanne

15/01/2024

Prof. Anastasios Vassilopoulos

Table of contents

1	Introduction	1
1.1	State of the art	1
1.1.1	Historical Perspective	1
1.1.2	Prosthetic Feet Categories	1
2	Preliminary Work	4
2.1	Modelling	4
2.2	Load Case	5
2.3	Materials	7
3	Methodology	9
3.1	Material's Constants and Compliance Matrix	9
3.2	Force and Moment Resultants	10
3.3	Mid-plane Strain and Curvatures	11
3.4	Failure Criteria	12
3.4.1	Maximum Stress Criterion	12
3.4.2	Tsai-Wu Criterion	12
3.4.3	Tsai-Hill Criterion	13
3.5	Optimization	13
4	Results and Validation	14
4.1	Classical Laminate Theory Results	14
4.2	Validation with Finite Element Analysis	16
4.2.1	Presentation and hypothesis	16
4.2.2	Materials	16
4.2.3	Stacking	17
4.2.4	Load Cases	17
4.2.5	Boundary Conditions	17
4.2.6	Symmetric Force Simulation	17
4.2.7	Asymmetric Force Simulation	18
4.2.8	Heel-off Simulation	18
4.2.9	Convergence Analysis and Validation of CLT	19
4.2.10	Results for a 110kg Patient	20
4.3	Design Optimization Results	21
4.3.1	Strength Ratio Maximization	21
4.3.2	Weight-to-Strength Ratio Minimization	24
4.4	Selected Design	25
5	Conclusion	26
5.1	Future Work	26
5.2	Code Availability	26
References		28

1 Introduction

Foot prostheses are crucial for people who've lost a part of their leg, helping them regain the ability to walk and carry out daily activities. These engineered solutions are especially important for those with transtibial amputations (below the knee) or transfemoral amputations (above the knee), compensating for the missing joints and enabling a smoother walking motion. Beyond physical support, prosthetic devices play a vital role in improving the mental well-being of amputees, restoring their independence and confidence by allowing them to move freely.

In our pursuit to enhance prosthetic feet, our project focuses on optimizing the orientation and arrangement of various carbon fiber-reinforced polymer laminae. These include both unidirectional and woven fabrics, carefully examining their impact on the overall performance of the prosthesis. Additionally, we explore the use of a core material positioned at the center of the laminate to decrease the cost and increase the stiffness. By strategically considering these factors, we aim to create a composite structure that maximizes the energy storage and return efficiency of the prosthetic foot. This involves utilizing classical lamination theory for stress and strain calculations within the laminate, incorporating various failure theories to ensure a reliable design with an appropriate factor of safety. Our optimization process, facilitated by a genetic algorithm implemented through MATLAB, seeks to identify the ideal configuration that achieves the highest strength ratio while minimizing weight and cost. Lastly, we validate our optimized prosthetic foot design using the finite element method, to confirm the structural integrity and performance of our proposed configuration.

1.1 State of the art

1.1.1 Historical Perspective

Prosthetic limbs have evolved significantly over the centuries. Early designs were basic, constructed from wood and metal, offering limited functionality and comfort. The first traces of prosthetic feet date back to ancient Egypt [1]. The advent of composite materials marked a turning point, enabling a shift from rigid constructions to more dynamic and lightweight prosthetics. This transition improved the overall quality of life for amputees, laying the foundation for the sophisticated prosthetic feet seen today. Carbon fiber-reinforced polymer (CFRP) laminates have become the cornerstone in prosthetic foot design due to their exceptional strength-to-weight ratio. Precise fiber orientation enhances structural integrity, contributing to improved walking dynamics and reduced user fatigue. While CFRP is dominant, alternatives such as glass fiber-reinforced polymers (GFRP) and composites incorporating natural fibers offer unique trade-offs between performance, cost, and sustainability.

1.1.2 Prosthetic Feet Categories

- Conventional Feet [2]:

Before the early 1980s, prosthetic feet primarily aimed to restore basic walking and simple occupational tasks. The SACH foot, standing for "Solid Ankle Cushioned Heel" was the industry standard, featuring a compressible heel wedge for pseudo-plantar flexion. The rigid wooden keel offered midstance stability but limited lateral movement. The simplicity and affordability of the SACH foot still make it a prevalent choice, especially in low-income countries.



Figure 1: Exemple of SACH feet [3]

- Energy Storing and Returning Feet [2]

The aspiration of amputees to engage in sports, coupled with the rigorous demands of athletic activities, has led to the creation of what is known as Energy Storing and Returning (ESR) feet. These specialized prosthetic feet can store energy during the stance phase and release it to assist amputees in forward propulsion during the late stance phase.

The introduction of the Seattle Foot in 1981 marked the debut of the first ESR foot. Within the Seattle Foot design, a flexible keel is situated within a polyurethane shell. This keel flexes under load, functioning as an elastic spring that later returns a portion of the stored energy to the amputee during the gait cycle.

A completely different prosthetic foot concept is commercially available since 1987. Flex-Foot Inc. came up with the Flex-Foot prosthesis with a flexible 100% carbon fiber shank and a heel spring. This device differs from others as it allows the entire prosthesis, rather than solely the foot part, to flex, store, and return energy to the amputee.



Figure 2: Exemple of ESR feet [4]

- Bionic Feet

In the realm of prosthetic research, a compelling third option is emerging, marked by the integration of bionic feet designed to replicate the entirety of human ankle behavior. Acknowledging the intricate characteristics of the human ankle and aiming for a comprehensive replication pose a unique design challenge for researchers. Unlike traditional approaches focused solely on ensuring energy return at specific moments in the gait cycle, this innovative perspective shifts the paradigm towards mimicking the total range of human ankle movements. By embracing this approach, prosthetic designers aspire to create bionic feet that not only provide enhanced functionality at crucial instances but also strive to emulate the intricate and dynamic behavior of the human ankle throughout the entire gait cycle. This nuanced consideration reflects a growing commitment to advancing prosthetic technology beyond isolated features, aiming for a more comprehensive and natural integration with the user's biomechanics. A bionic foot refers to a mechanical device with active components

designed for use by individuals with lower-limb amputations. Presently, the majority of developed bionic feet remain primarily in the realm of research, with only one prosthetic device having transitioned to commercialization. These devices can be classified according to their actuation principle into two main categories: those driven by pneumatic mechanisms and those propelled by electrical systems.



Figure 3: Exemple of bionic feet [5]

Figure 4 serves as a comprehensive recapitulation of the categorization of contemporary prosthetic feet, offering a visual representation of the diverse landscape in prosthetic technology. The diagram systematically organizes the various types of prosthetic feet based on their distinct characteristics and actuation principles.

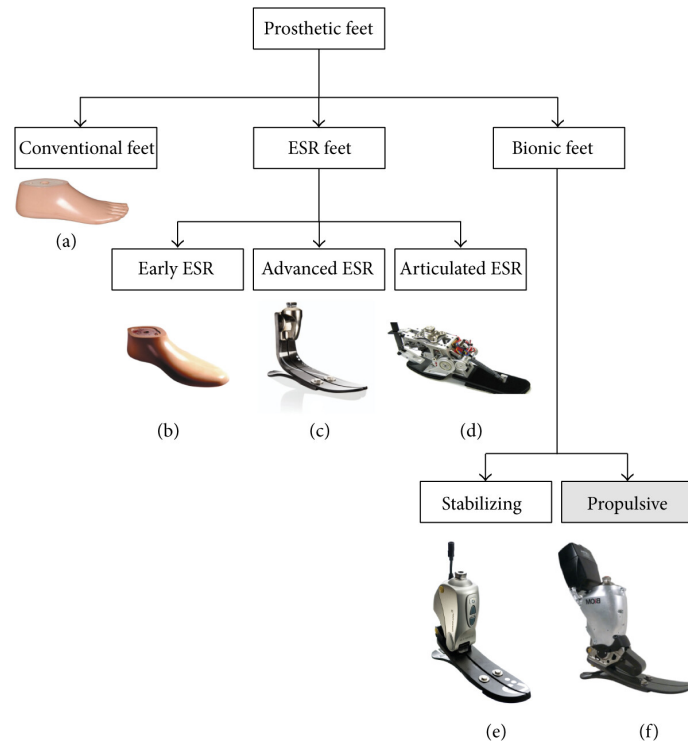


Figure 4: Categorization of today's prosthetic feet [6]

2 Preliminary Work

Before delving into the optimization of laminae orientation and arrangement, some preliminary work and assumptions are necessary. These include determining the prosthesis geometry, specifying the anticipated loads, identifying the most critical load case, and deciding on the materials for the optimization process.

2.1 Modelling

The composite energy-storing foot design modeling process involves a thorough examination of existing market products, with certain design modifications and simplifications for stress analysis on infinitesimal elements. Notably, commercial products often incorporate a toe-like gap to mitigate torsional effects at the foot's center. Additionally, a common feature observed in these products is the use of both a lower and an upper keel, connected either by screws or silicone. However, in our considerations, the holes have been eliminated, and the upper and lower keels are treated as a unified single composite structure.

In addressing the complexities of design curvatures, a simplified structure has been devised to facilitate stress calculations. The carbon foot design comprises four arcs, each characterized by specific radii as illustrated in Figure 5. To ensure scalability for different foot sizes, the total length of the foot is calculated using the shoe size, and every other dimension is scaled accordingly.

$$\text{Foot Length} = \frac{(\text{shoe size} - 2) \cdot 20}{3} \cdot 10^{-3} \text{mm} \quad (1)$$

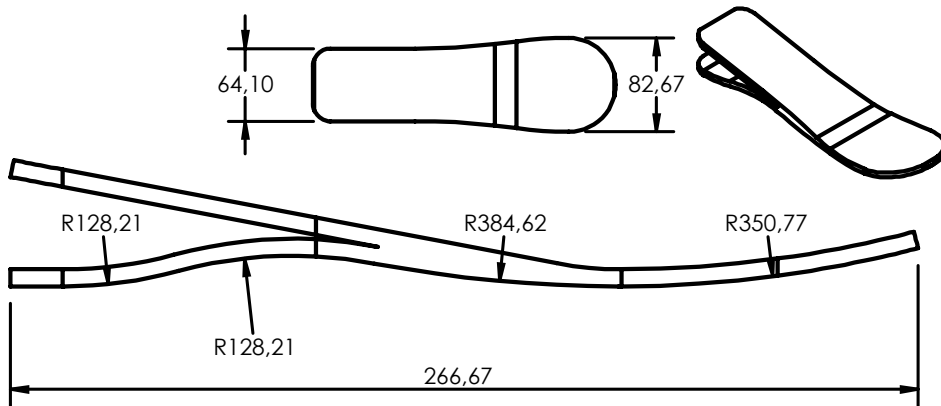


Figure 5: Our design for shoe size 42 after the simplifications on the commercial products.

The model is the largest foot size available with 26.67cm of length (EU-42) for a 55-110kg patient. The failure analysis of the model is performed for a 110kg patient with the largest foot size. A key assumption has been made regarding the fixation of the foot from the ankle joint, with the adaptor connecting the foot to the ankle considered rigid. This assumption provides a basis for analyzing the stress distribution within the composite structure. The overall design approach combines thoughtful adaptations from existing commercial models with deliberate simplifications to streamline stress analysis and enhance the feasibility of the composite energy-storing foot.

2.2 Load Case

The forces applied on the foot depend on lots of factors such as the weight and proportions of the person as well as the gait characteristics that can change from person to person. Moreover, the prosthetic gait of transfemoral or transtibial amputees is usually different from a healthy gait.[7] [8] In this study we assumed that the differences in forces caused by different gait characteristics are negligible. We have used a data set for a healthy gait obtained by David A. Winter [9]. This data set includes the positions of various markers on the legs and the ground reaction forces. All of the data is obtained using the gait of a person who weighs 56.7 kg. For the sake of simplicity, we assumed that the ground reaction forces would scale linearly with increasing weights. For the visualization of the gait and the ground reaction forces we have used MATLAB R2023b [10].

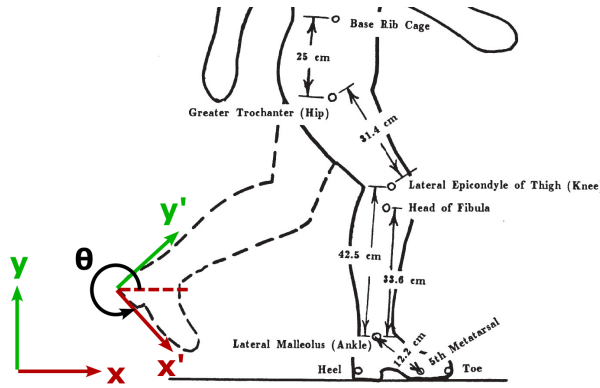


Figure 6: Marker locations and coordinate system information of the data set used in this study [9]

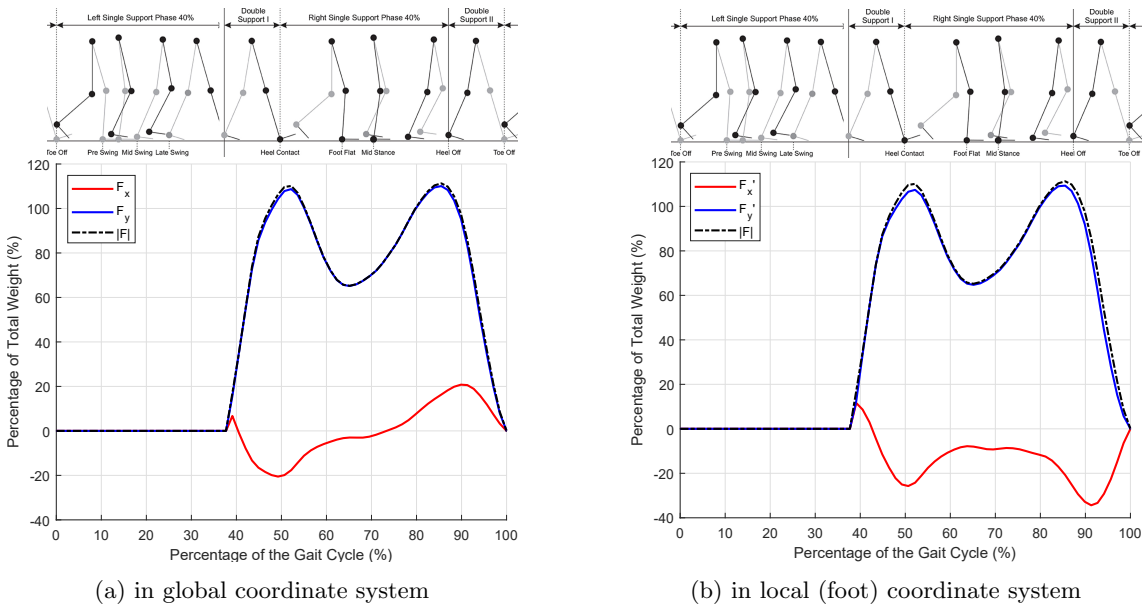


Figure 7: Ground reaction forces in global coordinate system during one gait cycle [9] [11]

To find the local forces acting on the foot we have performed a coordinate transform on the ground reaction forces and the center of pressure.

$$\begin{bmatrix} x' \\ y' \\ 1 \end{bmatrix} = \begin{bmatrix} R_{11} & R_{12} & P_{11} \\ R_{21} & R_{22} & P_{21} \\ 0 & 0 & 1 \end{bmatrix} \begin{bmatrix} x \\ y \\ 1 \end{bmatrix} \quad (2)$$

where

$$R = \begin{bmatrix} \cos(\theta) & -\sin(\theta) \\ \sin(\theta) & \cos(\theta) \end{bmatrix} \quad (3)$$

$$P = -R \cdot t \quad (4)$$

$$t = \begin{bmatrix} x_{heel} \\ y_{heel} \end{bmatrix} \quad (5)$$

We can see in Figure 7 that the maximum ground reaction forces, and therefore the greatest forces to be applied to the foot, occur during the heel contact and heel-off phases.

In addition, this data only provides ground reactions perpendicular and parallel to the foot. In our case, we have implemented forces in all three axes. Therefore, the ground reaction force parallel to the foot is divided into two components based on a natural human gait cycle. Depending on the walking speed and the habits of a person, the angle of the foot changes [12].

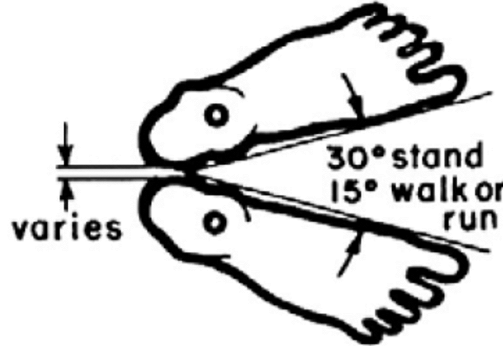


Figure 8: Typical angle between two feet while walking or running [12]

In our case, we have investigated walking or running cases with an angle of 15 degrees between feet. Also, in composite stress calculations, usually the z-axis is defined perpendicular to the composite whereas, the x-axis and y-axis are on the plane. To comply with the convention, we have defined the x-axis in the walking direction and the y-axis direction can be found from the cross product of z and x axes. Therefore, the following forces are obtained for each direction from the data.

$$F_x = F_x^* \cos(15^\circ) \quad (6)$$

$$F_y = F_x^* \sin(15^\circ) \quad (7)$$

$$F_z = -F_y \quad (8)$$

F_x^* and F_y^* represent the force data from the dataset obtained by David A. Winter [9] after transformation with Eqs. (1-4). The coordinate system based on the model can be seen in Figure 9.

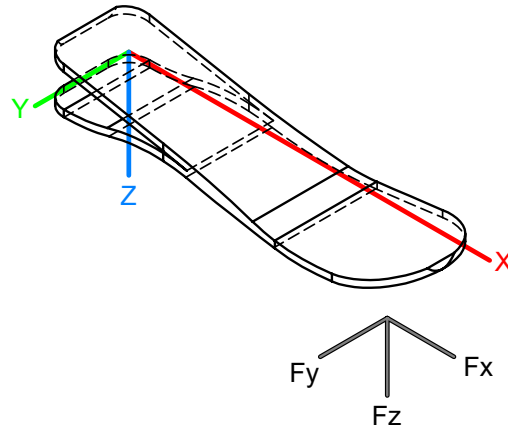


Figure 9: Coordinate system used for laminates and the applied forces on the model of the foot

2.3 Materials

This study aims to design a lightweight and possibly cheaper composite energy-storing foot. The three composites tested and presently being used in the composite industry are fiberglass, kevlar, and carbon fibers [13]. The selection of the material depends on the client. The activity and durability of the prosthesis are the highest with carbon fibers. However, fiberglass is the most common and economical composite. On the other hand, kevlar is the lightest and the most expensive composite. It is resistant to fracture and can absorb high loads of torque and stress while it is very poor in maintaining structure under load. Lastly, carbon is almost as light as kevlar and it is very stiff and able to hold its shape under stress. Therefore, carbon is the most used material among these three today since it provides the best performance. However, materials are changed based on the client's activity and cost optimization.

While designing a prosthetic foot, energy storage should also be considered. Even though glass fibers are very cheap and provide sufficient performance for inactive clients, the best performance in terms of energy storage can be achieved with carbon fibers [14]. In this study, we are going to aim for a higher-efficiency prosthetic foot for active patients. However, even though carbon fiber provides a very good performance, it is also very expensive. Therefore, in the experiments, we have also implemented a sandwich structure to reduce the design's cost. Also, both unidirectional and woven fabrics are used in the experiments to compare their performance.

Unidirectional fabrics have all the fibers oriented in the same direction and they can be laid down in multiple directions to achieve balanced mechanical properties. Since woven fabrics are weaved over and under each other creating slight bends on the fibers, performance is reduced. Also, woven fabrics go over more processing to weave them together, which increases the cost and degrades the performance. On the other hand, damage tolerance, machinability, and tolerance to crack growth of woven fabrics are better than that of unidirectional fabrics. It is common to use both fabrics together in a design where the unidirectional fabrics are placed inside to generate the highest strength and the woven fabrics are placed outside to improve damage tolerance and machinability.

We used a unidirectional and woven fabric with or without Rohacell core to experiment with sandwich structures for the design. This core material was chosen instead of Airex because it is more waterproof and more resistant, two characteristics necessary for the durability (weather conditions) and efficiency of the structure. The material properties are listed in Table 2.

Material properties are taken from Altair EsaCOMP[15] software through the EPFL license. Properties of the used materials can be found in the following tables.

Table 1: Parameters of fabrics.

(a) Parameters of Cycom 381 IM7 unidirectional fabric.

Property	Value	Unit
E_1	156	GPa
E_2	8.83	GPa
E_3	8.83	GPa
G_{12}	4.34	GPa
G_{13}	3.39	GPa
G_{23}	4.30	GPa
v_{13}, v_{23}, v_{13}	0.3	
ρ	1583	kg/m ³
$\sigma_{T,1}$	2468	MPa
$\sigma_{C,1}$	1482	MPa
$\sigma_{T,2}$	38	MPa
$\sigma_{C,2}$	176.6	MPa
σ_{66}	128	MPa
t	0.142	mm

(b) Parameters of Carbone TWILL woven fabric.

Property	Value	Unit
E_1, E_2	60.4	GPa
E_3	36	GPa
G_{12}	4.27	GPa
G_{13}	3.50	GPa
G_{23}	3.50	GPa
v_{13}, v_{23}	0.35	
v_{13}	0.30	
ρ	1495	kg/m ³
$\sigma_{T,1}$	361.7	MPa
$\sigma_{C,1}$	294.6	MPa
$\sigma_{T,2}$	361.7	MPa
$\sigma_{C,2}$	294.6	MPa
σ_{66}	68.9	MPa
t	0.25	mm

Table 2: Parameters of isotropic Rohacell core.

Property	Value	Unit
E	60.4	GPa
G	22.37	GPa
v	0.35	
ρ	1495	kg/m ³
t	5	mm

From the tables, it can be observed that the mechanical properties of the core are worse than the fabrics. However, by creating a sandwich structure the mechanical properties can be enhanced with a cheaper and a more light-weight design. Both bidirectional and unidirectional fabrics are implemented in the experiments and their combination in a sandwich structure is also examined.

3 Methodology

In this section, all the calculations are performed using MATLAB R2023b to ease the calculations and to create visualizations of the results.

In addition, in the calculations classical laminate theory (CLT) is used; therefore, the following assumptions are made.

- The length and the width of the plate are much larger than the thickness of the plate.
- The deformation is completely described by the transverse deflection of the middle surface plane.
- Line elements lying perpendicular to the middle surface of the plate remain perpendicular to the middle surface during deformation.
- Line elements lying perpendicular to the mid-surface do not change length during deformation.
- No out-of-plane loads.

3.1 Material's Constants and Compliance Matrix

Initially, the compliance and stiffness matrix is calculated. Since the composite is assumed to be thin, reduced compliance and stiffness matrices are calculated.

$$S = \begin{bmatrix} S_{11} & S_{12} & 0 \\ S_{12} & S_{22} & 0 \\ 0 & 0 & S_{66} \end{bmatrix}, \quad Q = S^{-1} \quad (9)$$

Where each matrix element can be calculated as follows.

$$\begin{aligned} S_{11} &= 1/E_1 \\ E_{12} &= -v_{12}/E_1 \\ S_{22} &= 1/E_2 \\ S_{66} &= 1/G_{12} \end{aligned}$$

Then, for off-axis stresses, transformed reduces compliance and stiffness matrices are calculated using the transformation matrix. For any rotation of angle θ , the rotation matrix (T) and the Reuter matrix (R) can be calculated as follows.

$$T = \begin{bmatrix} \cos^2(\theta) & \sin^2(\theta) & 2\sin(\theta)\cos(\theta) \\ \cos^2(\theta) & \sin^2(\theta) & -2\sin(\theta)\cos(\theta) \\ -\sin(\theta)\cos(\theta) & \sin(\theta)\cos(\theta) & \cos^2(\theta) - \sin^2(\theta) \end{bmatrix}, \quad R = \begin{bmatrix} 1 & 0 & 0 \\ 0 & 1 & 0 \\ 0 & 0 & 2 \end{bmatrix} \quad (10)$$

The angle transformations can be made through the following compliance and stiffness matrices calculations.

$$\bar{Q} = T^{-1} Q R T R^{-1}, \quad \bar{S} = \bar{Q}^{-1} \quad (11)$$

After calculating the stiffness and compliance matrices, extensional, coupling and flexural stiffness matrices can be calculated from the following formulas.

$$A_{ij} = \sum_{k=1}^n \bar{Q}_{ij}^{(k)} (z_k - z_{k-1}) \quad (12)$$

$$B_{ij} = \frac{1}{2} \sum_{k=1}^n \bar{Q}_{ij}^{(k)} (z_k^2 - z_{k-1}^2) \quad (13)$$

$$D_{ij} = \frac{1}{3} \sum_{k=1}^n \bar{Q}_{ij}^{(k)} (z_k^3 - z_{k-1}^3) \quad (14)$$

Then, constitutive equations for a general laminate can be written with the found matrices as follows.

$$\begin{bmatrix} N \\ M \end{bmatrix} = \begin{bmatrix} A & B \\ B & D \end{bmatrix} \begin{bmatrix} \varepsilon \\ \kappa \end{bmatrix} \quad (15)$$

3.2 Force and Moment Resultants

The force and moment resultants are calculated on the weakest part of the foot. According to our design, it corresponds to the point closest to the ankle joint. This is because the moment arm is maximum on the differential element considered when the max force in the gait is generated at the toe. Also, it is because of the arched geometry in the fixed position. Therefore, force and moment resultants can be calculated from the following formulas.

$$\begin{Bmatrix} N_x \\ N_y \\ N_{xy} \end{Bmatrix} = \int_{-H/2}^{H/2} \begin{Bmatrix} \sigma_x \\ \sigma_y \\ \tau_{xy} \end{Bmatrix} dz \quad \begin{Bmatrix} M_x \\ M_y \\ M_{xy} \end{Bmatrix} = - \int_{-H/2}^{H/2} \begin{Bmatrix} \sigma_x \\ \sigma_y \\ \tau_{xy} \end{Bmatrix} z dz \quad (16)$$

Where H describes the total thickness of the composite. In our case, stresses on the differential element can be formulated as follows.

$$\sigma_x = \frac{F_x}{H \cdot a} + \frac{F_y \cdot b \cdot a}{2I_z} + \frac{F_z \cdot b \cdot (z - e)}{H \cdot a \cdot e \cdot (R - z + e)} \quad (17)$$

$$\sigma_y = \frac{F_y}{H \cdot b} \quad (18)$$

$$\tau_{xy} = \frac{F_y}{H \cdot a} + \frac{F_z \cdot a}{2J} \sqrt{z^2 + a^2/4} \quad (19)$$

In the equations, a is the width of the foot, b is the distance from the point of interest to the force, R is the radius of the curved region of interest and e is the difference between the natural

axis and the centroid of the beam. Other parameters are I_y , I_z , and J which correspond to the area moment of inertia around y, z, and polar moment of inertia, respectively.

For σ_x , the first part represents the stress caused by the force F_x , the second part indicates the bending stress from F_y , and the last part reflects the bending stress on the curved section from F_z . In the case of σ_y , the stress is simply derived from F_y as it is the sole contributing component. Regarding τ_{xy} , the initial part signifies the shear stress from F_y , while the second part represents the torsional stress from F_z .

After the integrations, force and moment components are found as follows.

$$\begin{aligned} N_x &= \frac{F_x}{a} + \frac{F_y \cdot b \cdot a \cdot H}{2I_z} + \frac{F_z \cdot b}{H \cdot a \cdot e} \cdot (R \ln((R + H/2 + e)/(R - H/2 + e)) - H) \\ N_y &= \frac{F_y}{b} \\ N_{xy} &= \frac{F_y}{a} \\ M_x &= \frac{F_z \cdot b}{2H \cdot a \cdot e} \cdot (2H \cdot R + 2R \cdot (R + e) \cdot \ln((R - H/2 + e)/(R + H/2 + e))) \\ M_y &= 0 \\ M_{xy} &= \frac{F_z \cdot a^4}{16J} \left(-1/4 \cdot \left(\frac{H}{a} \cdot \sqrt{1 + \frac{H^2}{a^2}} + 1/2 \ln \left(\frac{\left| \frac{H}{a} + \sqrt{1 + \frac{H^2}{a^2}} \right|}{\left| -\frac{H}{a} + \sqrt{1 + \frac{H^2}{a^2}} \right|} \right) \right) \right) + \frac{H}{2a} \left(1 + \frac{H^2}{a^2} \right)^{1.5} \end{aligned}$$

3.3 Mid-plane Strain and Curvatures

Mid-plane strains and curvatures can be found by solving the Eq. 15. After finding mid-plane strains and curvatures, strains for each point of the laminate can be found by:

$$\begin{Bmatrix} \varepsilon_x \\ \varepsilon_y \\ \gamma_{xy} \end{Bmatrix} = \begin{Bmatrix} \varepsilon_x^0 \\ \varepsilon_y^0 \\ \gamma_{xy}^0 \end{Bmatrix} + z \cdot \begin{Bmatrix} \kappa_x \\ \kappa_y \\ \kappa_{xy} \end{Bmatrix} \quad (20)$$

The stress state for each lamina can be found by using the reduced stiffness matrix for that lamina:

$$\begin{Bmatrix} \sigma_x \\ \sigma_y \\ \tau_{xy} \end{Bmatrix} = \bar{Q} \cdot \begin{Bmatrix} \varepsilon_x \\ \varepsilon_y \\ \gamma_{xy} \end{Bmatrix} \quad (21)$$

To find the local stresses in every lamina, we can use the rotation matrix defined in equation 10.

$$\sigma_{\text{local}} = \begin{Bmatrix} \sigma_1 \\ \sigma_2 \\ \tau_{12} \end{Bmatrix} = T \cdot \begin{Bmatrix} \sigma_x \\ \sigma_y \\ \tau_{xy} \end{Bmatrix} \quad (22)$$

3.4 Failure Criteria

Three failure criteria are employed to estimate the strength ratio of our design. To ensure a safe design, the minimum safety ratio is considered as the actual strength ratio in the optimization procedure.

3.4.1 Maximum Stress Criterion

According to maximum stress theory, the failure will occur if one of the inequalities shown in equations 23, 24, and 25 is violated.

$$-(\sigma_1^C)_{ult} < \sigma_1 < (\sigma_1^T)_{ult} \quad (23)$$

$$-(\sigma_2^C)_{ult} < \sigma_2 < (\sigma_2^T)_{ult} \quad (24)$$

$$-(\tau_{12})_{ult} < \tau_{12} < (\tau_{12})_{ult} \quad (25)$$

For a known local stress state, the strength ratio can be calculated as:

$$R = \min \left(\frac{(\sigma_1^T)_{ult}}{\sigma_1}, \frac{-(\sigma_1^C)_{ult}}{\sigma_1}, \frac{(\sigma_2^T)_{ult}}{\sigma_2}, \frac{-(\sigma_2^C)_{ult}}{\sigma_2}, \frac{(\tau_{12})_{ult}}{\tau_{12}} \right) \quad (26)$$

3.4.2 Tsai-Wu Criterion

According to Tsai-Wu criterion[16], the lamina is considered to be failed if this inequality is satisfied:

$$H_1\sigma_1 + H_2\sigma_2 + H_6\tau_{12} + H_{11}\sigma_1^2 + H_{22}\sigma_2^2 + H_{66}\tau_{12}^2 + 2H_{12}\sigma_1\sigma_2 < 1 \quad (27)$$

Coefficients can be determined by considering the simple loading cases.

$$H_1 = \frac{1}{(\sigma_1^T)_{ult}} - \frac{1}{(\sigma_1^C)_{ult}} \quad (28)$$

$$H_{11} = \frac{1}{(\sigma_1^T)_{ult} \cdot (\sigma_1^C)_{ult}} \quad (29)$$

$$H_2 = \frac{1}{(\sigma_2^T)_{ult}} - \frac{1}{(\sigma_2^C)_{ult}} \quad (30)$$

$$H_{22} = \frac{1}{(\sigma_2^T)_{ult} \cdot (\sigma_2^C)_{ult}} \quad (31)$$

$$H_6 = 0 \quad (32)$$

$$H_{66} = \frac{1}{(\tau_{12})_{ult}^2} \quad (33)$$

For the remaining parameter, an empirical suggestion by Mises-Hencky [17] can be used:

$$H_{12} = -\frac{1}{2} \sqrt{\frac{1}{(\sigma_1^T)_{ult} \cdot (\sigma_1^C)_{ult} \cdot (\sigma_2^T)_{ult} \cdot (\sigma_2^C)_{ult}}} \quad (34)$$

For a known local stress state, the strength ratio can be calculated as the minimum root of the following polynomial:

$$(H_{11}\sigma_1^2 + H_{22}\sigma_2^2 + H_{66}\tau_{12}^2 + 2H_{12}\sigma_1\sigma_2)R^2 + (H_1\sigma_1 + H_2\sigma_2 + H_6\tau_{12})R - 1 = 0 \quad (35)$$

3.4.3 Tsai-Hill Criterion

According to Tsai-Hill criterion[18], the lamina is considered to be failed if this inequality is satisfied:

$$H_{11}\sigma_1^2 + H_{22}\sigma_2^2 + H_{66}\tau_{12}^2 + 2H_{12}\sigma_1\sigma_2 < 1 \quad (36)$$

where

$$H_{11} = \frac{1}{(\sigma_1^T)^2_{ult}} \quad (37)$$

$$H_{22} = \frac{1}{(\sigma_2^T)^2_{ult}} \quad (38)$$

$$H_{12} = -\frac{1}{2(\sigma_1^T)^2_{ult}} \quad (39)$$

$$H_{66} = \frac{1}{(\tau_{12})^2_{ult}} \quad (40)$$

For a known local stress state, the strength ratio can be calculated as the minimum root of the following polynomial:

$$(H_{11}\sigma_1^2 + H_{22}\sigma_2^2 + H_{66}\tau_{12}^2 + 2H_{12}\sigma_1\sigma_2)R^2 - 1 = 0 \quad (41)$$

3.5 Optimization

The optimized design is aimed at the most critical case. Initially, commercial products in the market are investigated. It is observed that usually, the largest foot size offered in the market is around 26cm (EU-42) and the largest body weight supported by the designs is 110kg. Therefore, as discussed in the modeling part, the design is optimized for a 26cm length foot and a 110kg patient.

There are some initial considerations and constraints in the optimization. Firstly, to avoid buckling after the curing process, a symmetric laminate is considered for both upper and lower kneels. Secondly, a high strength ratio (SR) is desirable. However, a too-large SR might decrease the energy-storing ability of the design for lighter patients since the design will be too stiff and the gait will be too uncomfortable. Therefore, a minimum SR of 3-3.5 is desirable for the most critical case. Additionally, the weight of the design should be minimized. Therefore, in optimization, two different composites and core materials are introduced that minimize weight to strength ratio. Lastly, in most commercial products the thickness of the lower kneel is close to half of the thickness of the upper kneel. Therefore, the design optimization is constrained such that the thickness of the lower kneel is half of the thickness of the upper kneel.

In addition, the energy-storing aspect of the prosthesis should be calculated with strain energy-based methods. Therefore, it cannot be investigated with CLT. Since the optimization is based on stress and strain calculations using CLT, the energy-storing aspect of the foot is investigated depending on previous research. As investigated by Jiang[19], the tensile energy stored by the foot prosthesis increases as the number of cross plies increases. The effect mentioned in this paper is shown as a result of the increase in laminate stiffness. As explained by Segal et al., energy storing and return effects on a prosthetic foot decrease the net metabolic energy cost of gait, thus increasing the quality of life of the patient.[20] In some of the design experiments, to put a lower limit on the stored strain energy, we added a constraint to the optimization that the number of cross-ply laminates ($\pm 45^\circ$) should not be less than 25% of the total number of laminates.

Then, we optimized the layer count for a quasi-isotropic design, a sandwich structure design, and a design constrained only with cross-ply lamination. Finally, we have implemented an optimization

problem that selects the optimum material, lamina orientation, and core thickness for a given laminate count and minimizes the weight-to-strength ratio. Then, we removed the addition of the core and considered an optimization problem that selects the material and lamina orientation by maximizing SR for a given lamina count.

The strength ratio for the prosthetic feet is considered for two cases. Either with ground reaction forces applied from the inner region of the foot or the outer region of the foot. In each case, the critical region is investigated throughout the gait, and the minimum strength ratio calculated from the three failure criteria is to be maximized. Therefore, the most conservative design is obtained.

The optimization is performed on MATLAB R2023b using a genetic algorithm. In the algorithm, the lamina count is changed in each iteration and the optimum layer sequence is found by optimizing the given problem.

4 Results and Validation

In this section, we first present the results of classical lamination theory calculations for a given configuration. Subsequently, the identical configurations undergo analysis using the finite element method, serving to validate the accuracy of the CLT calculations. Finally, an optimization process based on CLT calculations is conducted to identify the optimal stacking configuration for our application.

4.1 Classical Laminate Theory Results

As the structure is fairly working in the longitudinal axis (the direction 0°), it is convenient to use a UD textile. This is because the structure is mainly loaded in one direction, it is better to use a material that has high mechanical properties in the principal direction rather than two directions with lower properties. However, in the initial design, we tried to implement a quasi-isotropic design. Further considerations about the layer sequence will be made in the optimization part. The results of the failure index (FI) are also reported as it will be compared with FEA results in the next part.

The following configuration is used in this section:

- **Upper kneel** using UD ply: $[0_3/45/90/-45]_{4s}$; a total of 48 layers
- **Lower kneel** using UD ply: $[0_5/45/90/-45]_{2s}$; a total of 32 layers

For this configuration mass and strength ratio values are found as:

- Total mass: 238.10 g
- Minimum strength ratio: 8.66
- Minimum strength ratio (Max Stress): 9.42 (FI = 0.106)
- Minimum strength ratio (Tsai-Wu): 8.66 (FI = 0.116)
- Minimum strength ratio (Tsai-Hill): 9.26 (FI = 0.108)

In Figure 10, the distributions of strain, stress, and strength ratio within the laminate are illustrated for the most critical timestep in the gait, identified as the heel-off phase. As depicted in Figure 10b, the primary stress component, σ_x , aligns predominantly with the 0° laminae, while σ_y and τ_{xy} are distributed across other laminae. Figure 10c presents the strength ratio distribution

in the laminate, indicating that laminae with lower strength ratio values are more susceptible to failure.

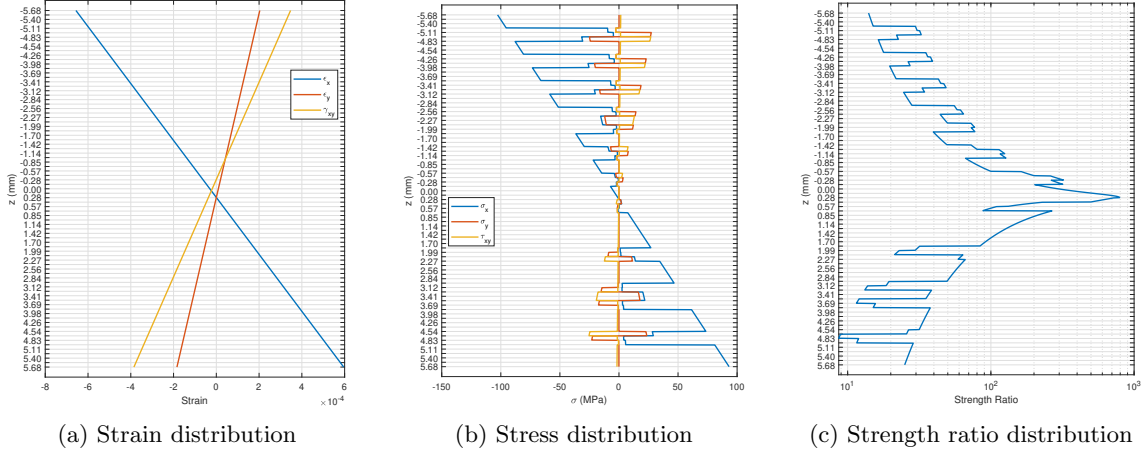


Figure 10: Strain, stress, and strength ratio distributions in the laminate for the most critical time-step.

Figure 11, shows the minimum strength ratio throughout the stance phase. As expected at the beginning of the stance gait, the strength ratio is larger since the foot does not support all the weight of the patient yet. The strength ratio decreases and makes a local minimum at about 20% of the gait. The global minimum is at about 80% of the gait, which corresponds to the toe-off phase. The global minimum occurs at the heel-off phase as expected since the foot supports all of the body weight and an additional ground reaction force is added due to acceleration.

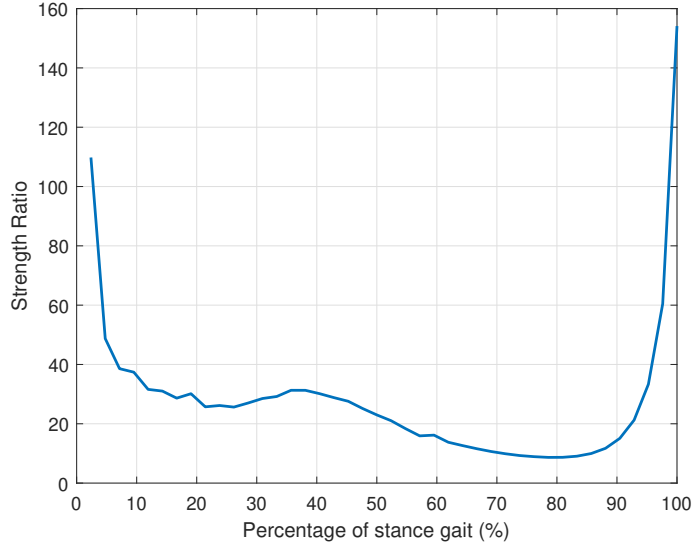


Figure 11: Evolution of strength ratio over time for one stance gait

As can be observed from the SR results provided, in each case and for every criterion, the

design is too safe. This can also be observed from the following plots. The strength ratio should be optimized to decrease the stiffness of the design to provide a more comfortable gait.

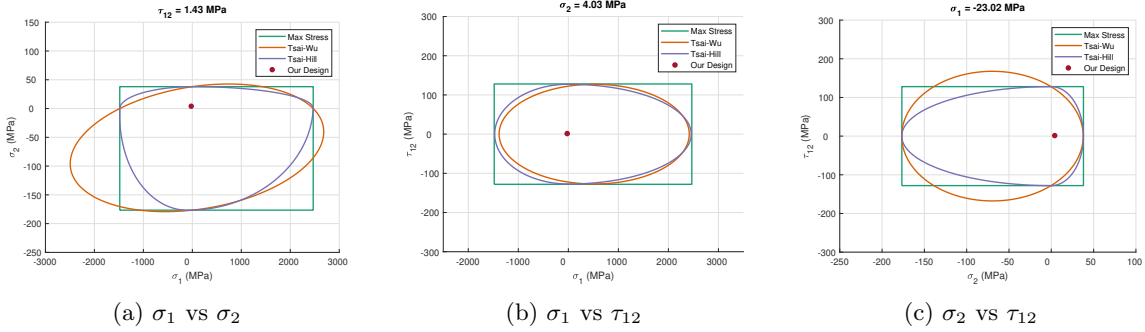


Figure 12: Failure loci for different failure criteria and our design

4.2 Validation with Finite Element Analysis

4.2.1 Presentation and hypothesis

To simulate the foot prosthesis, Figure 13a, several hypotheses have been considered. It is crucial to emphasize that the structural elements incorporated into the simulation consist solely of the upper keel and the lower kneel of the foot prosthesis, as depicted in Figure 13b. In contrast to the details outlined in Section 2.1, the analysis now encompasses the inclusion of holes for the top three screws, along with the two holes facilitating attachment between the two parts (located at the center of the foot).



(a) General assembly of the foot prosthesis CAD (b) Geometry of the foot prosthesis.

Figure 13: CAD and geometry of the foot prosthesis.

4.2.2 Materials

As mentioned, the structure will be made of composite materials, which means it is composed of different materials such as carbon fibers, epoxy resin, and foam to make a sandwich structure. In the following sections, the study will present the results for 2 different cases. A sandwich structure and a monolithic structure; to observe the benefit aspect of the foam. In Section 2.3, it is said that there exist different types of textiles composed of fibers.

In the finite element analysis, CLT results are validated. Therefore, the same configuration with the UD fibers is used in FEM. Also, to compare the foam and observe the effect of adding

foam on the performance, additional results are presented for a sandwich structure for optimization considerations.

4.2.3 Stacking

The stacks were determined using the Matlab coding to be then verified with finite element modeling. In fact, with the load cases presented in the following sections, the optimized stacking is to be chosen for the 2 parts of the structure to resist all possible situations, but with a reasonable weight of the structure. In this analysis, the same stacking is used with the CLT calculations. The detailed stacking is the following one with or without the foam for the 2 cases.

- **Upper kneel** using UD ply (and foam) : $[0_3/45/90/-45]_{4s}$; a total of 48 layers
- **Lower kneel** using UD ply (and foam) : $[0_5/45/90/-45]_{2s}$; a total of 32 layers

These sequences have a symmetric plane and have respectively 50% and 62,5% of the fiber in the principal direction to withstand the load cases.

4.2.4 Load Cases

As the foot prosthesis will be used by people every day to walk or run, it is important to know whether it will withstand all the possible load cases that it may be subjected to. This product is designed for patients of 50kg to 110kg. In finite element analysis, the validation is performed for a 70kg patient and additional results are provided for the most critical case of 110kg for further optimization. To have an idea about the optimization constraints, in addition to normal bending forces, a torsion case is also considered by applying force from one side of the foot as was done in CLT calculations.

4.2.5 Boundary Conditions

For each of the following cases, the same boundary conditions are applied. Indeed, as it can be seen in Figures 14, 15, and 16 the structure is embedded at three different points. These points correspond to the structural parts where the foot prosthesis is attached with the screws to the rest. They are represented by the blue-shaded region in the figure below. At these points, any movement in the x, y, and z directions or any rotation is blocked. Furthermore, a tie has been established between the lower and upper sections at the contact zone.

4.2.6 Symmetric Force Simulation

As outlined in Section 2.2, the ground reaction force undergoes variations throughout the foot's movement. In this context, the maximum load case pertains to the front part of the foot, where 110% of the weight (121 kg) is concentrated at a distance of 30 cm from the tip of the foot prosthesis. Consequently, the applied resultant force is $F_z = 1188$ N.

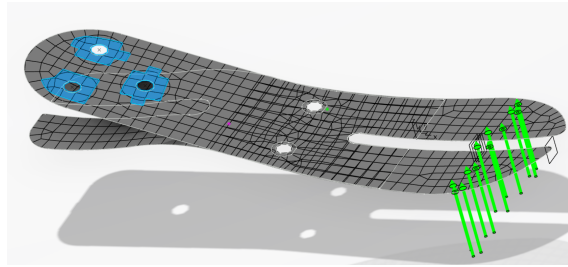


Figure 14: FEA Geometry for the front load case weight.

4.2.7 Asymmetric Force Simulation

This load case is similar to the previous one ($F_z = 1188N$), with the distinction lying in the applied zone, as illustrated in Figure 15. In this scenario, we account for a varied contact surface of the foot, acknowledging the diverse walking or running styles individuals may have, including pronation and supination. Consequently, this variation necessitates the foot prosthesis to operate under torsional forces, thereby justifying the incorporation of secondary directions in the composite sequence.

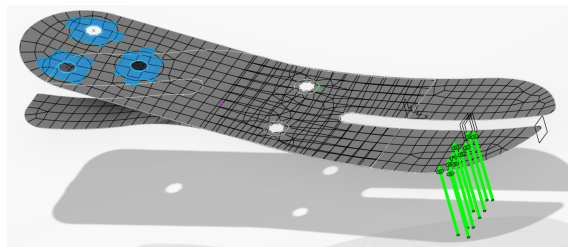


Figure 15: FEA Geometry for the torsion load case.

4.2.8 Heel-off Simulation

In this ultimate load case, we consider the most severe ground reaction applied at the base of the foot prosthesis, on the lower surface experiencing the same force magnitude as the initial load case ($F_z = 1188 N$). This simulation is done since the lower knee and upper knee are not in contact at this phase of the gait which might create a critical situation in the gait.



Figure 16: FEA Geometry for the bottom load case.

4.2.9 Convergence Analysis and Validation of CLT

To be sure that the results are convenient and that the mesh is well optimized, it is important to verify that the results do not depend on the size of the mesh.

For this analysis, a quadratic element type has been chosen. Indeed, there are holes inside the design, which will be better approximated with the help of quadratic elements rather than linear ones. This will also make the mesh more homogeneous, which is important. The element type has been set to quadratic to allow faster and more accurate convergence than for linear elements.

To optimize the mesh, a convergence analysis has been made on the upper and lower kneel, simultaneously. To validate the CLT calculations, this analysis is done on the normal load case for a person of 70kg $F_z = 755N$. Initially, a mesh of size $h = 5$ mm is applied. Then, the mesh was decreased to achieve the convergence. The results of the convergence analysis are recapitulated in a table and the convergence can also be seen in different graphs. The calculated values are the Tsai-Hill and Tsai-Wu criteria and the displacement of the structure (U). With Table 3 it is possible to remark that the final value for the mesh size is 3 mm for the upper and lower part. The convergence value is achieved if the error concerning the reference value is smaller than 2 %, Figure 18. The convergence can also be seen with the help of Figure 17.

Table 3: The results of the convergence analysis for the sled.

Mesh's size [mm]	TSAIW	TSAIH	U [mm]	Error TSAIW	Error TSAIH	Error U
5	0,137	0,46	5,04	5,52	5,19	0,20
4	0,139	0,154	5,02	4,14	0	0,59
3	0,145	0,155	5,06	0	0,65	0,20
2	0,146	0,153	5,04	0,69	0,65	0,20
1	0,145	0,154	5,05	0	0	0

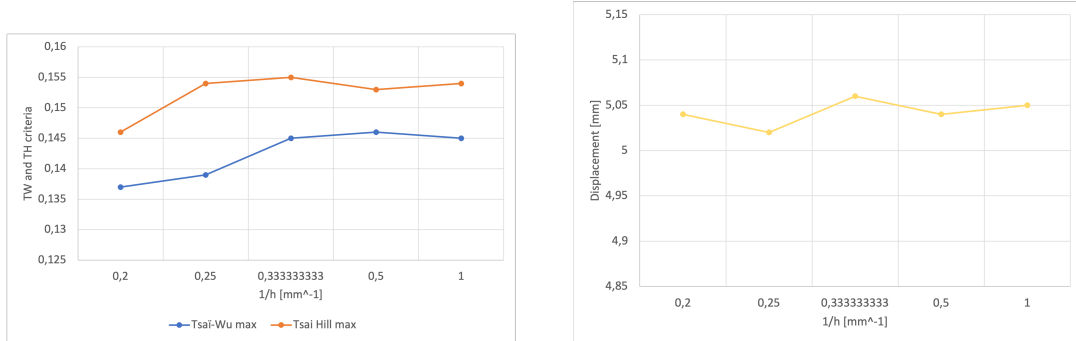
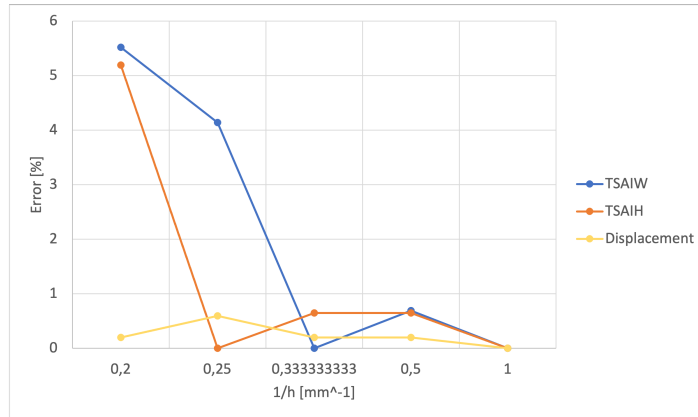


Figure 17: The convergence of TSAIH, TSAIW, and of the displacement as a function of $1/h$ for the normal load case.

Figure 18: The error as a function of $1/h$ for the sled.

The SR results for Tsai-Wu and Tsai-Hill criteria are also given in Table 3. It can be observed that there is a small difference between the results of CLT calculations. This is mainly because in CLT calculations we cannot consider out-of-plane loads. In this case, however, τ_{xz} is an important component of the stress calculations. Therefore, it creates a small difference. Finally, other assumptions about the plane theory create small differences in SR results.

4.2.10 Results for a 110kg Patient

Symmetric Load Case

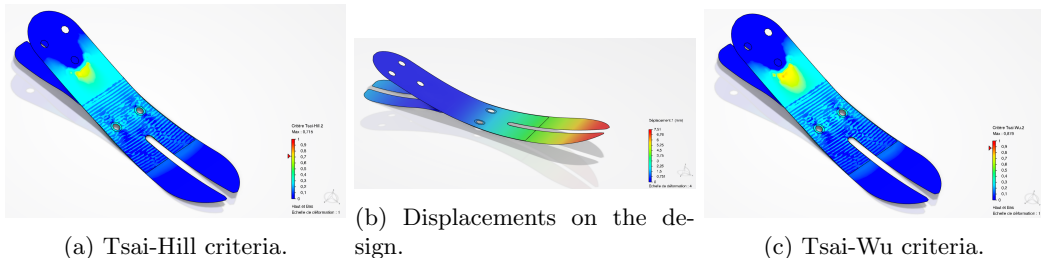


Figure 19: Monolithic structure case.

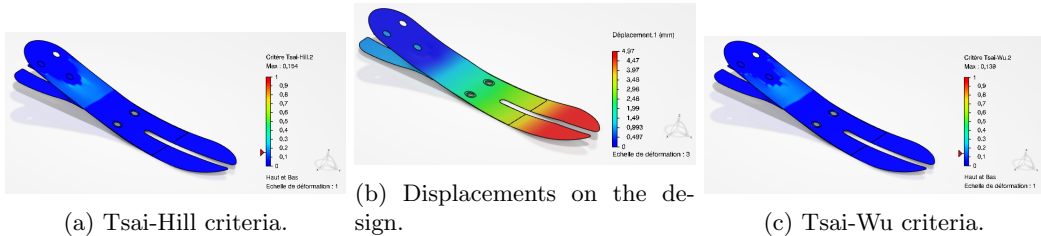


Figure 20: Sandwich structure case.

Asymmetric Load Case

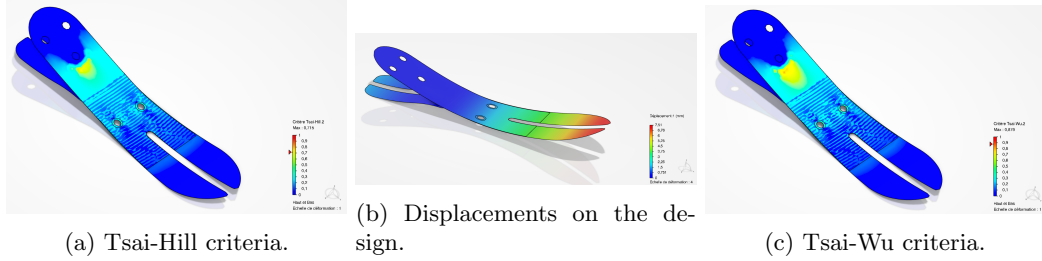


Figure 21: Monolithic structure case.

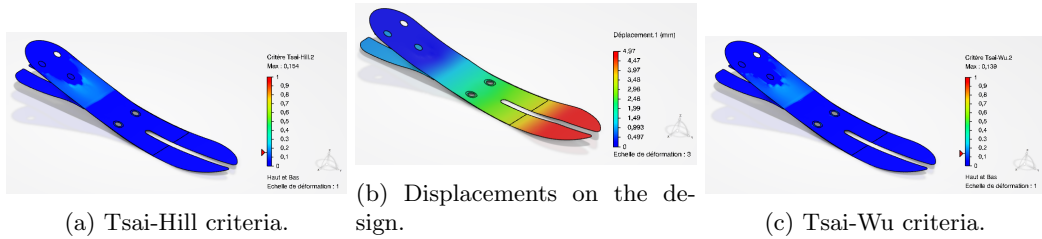


Figure 22: Sandwich structure case.

Heel-off Case

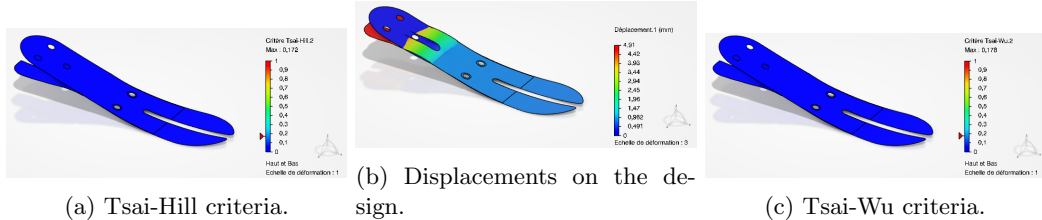


Figure 23: Sandwich structure case.

4.3 Design Optimization Results

The experiments with quasi-isotropic design significantly decreased the performance of the design. The main results we are going to present are based on the maximum SR obtained for a given laminate size and the maximum weight-to-SR ratio obtained for a sandwich structure. In the second problem, the optimization algorithm is set free to select if there will be a sandwich structure or not. This problem is investigated to understand if implementing a sandwich structure is reasonable.

4.3.1 Strength Ratio Maximization

In this optimization, varying numbers of laminae and two distinct materials are considered to calculate the maximum strength ratio. The optimization process determines the optimal laminae

sequence and material combination that yields the highest strength ratio. Notably, the optimization excludes the use of core material.

Here, optimization resulted in selecting Cycom 381 UD plies. The change in the weight and SR is plotted in Figure 24. Here, since the most critical case of 110kg with the largest foot size is examined an SR between 3 to 3.5 is to be obtained. This SR interval is aimed at the design since there are fatigue considerations in the life cycle of the product and we do not want the design to be too stiff to provide a comfortable gait for all weights between 50kg to 110kg.

In addition, to perform the optimization in such a large range of layers, the population size is decreased and function tolerance is increased in the genetic algorithm options. Therefore, a global optimum might not be found in Figure 24. In the next part, we shrank the interval increased population size, and decreased function tolerance to find the optimum design.

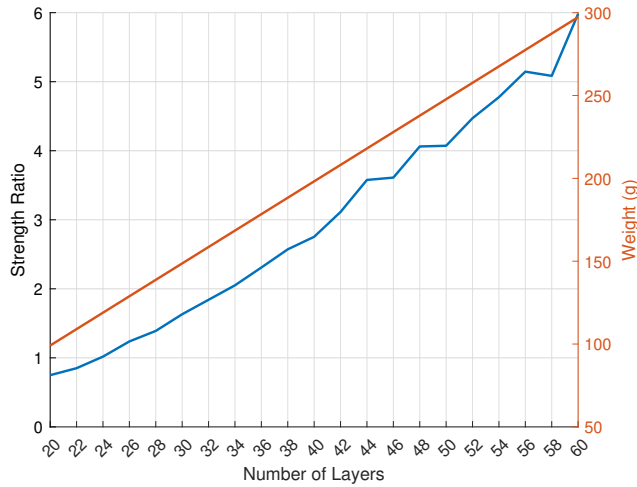


Figure 24: Optimization results for each lamina count.

For the next part, we have decided to find the optimum design in the interval of 36-46 layers. As an example, the following configuration is obtained from the optimization for 44 layers and a strength ratio of 3.20:

- **Upper kneel** using UD ply: $[0, 0, 0, 0, 0, 0, 0, 0, 0, 0, -45, 90, 90, 45]_s$; a total of 30 layers
- **Lower kneel** using UD ply: $[0, 0, 0, 0, -45, 45, 0]_s$; a total of 14 layers

In Figure 25, the distributions of strain, stress, and strength ratio within the laminate are illustrated for the most critical timestep in the gait, identified as the heel-off phase.

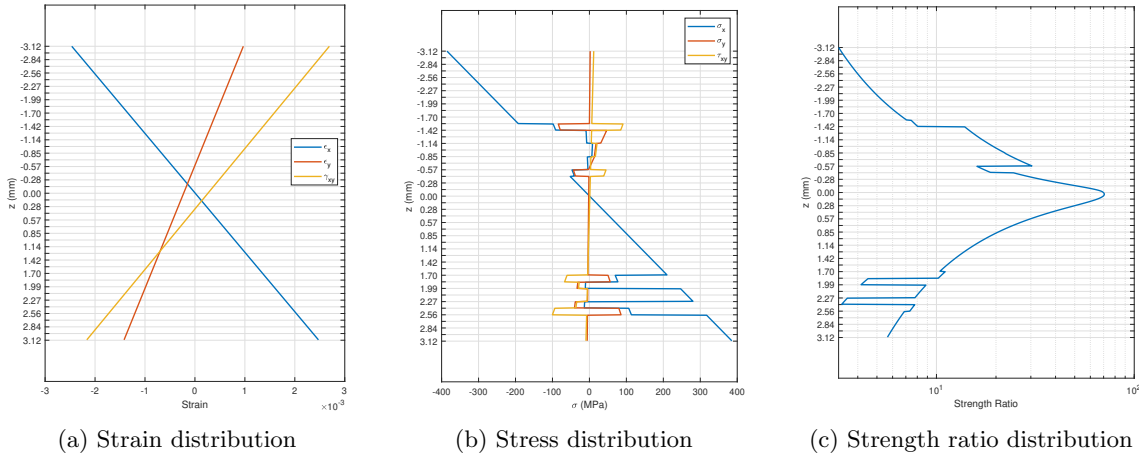


Figure 25: Strain, stress, and strength ratio distributions in the laminate for the most critical timestep.

Figure 26, shows the minimum strength ratio throughout the stance phase.

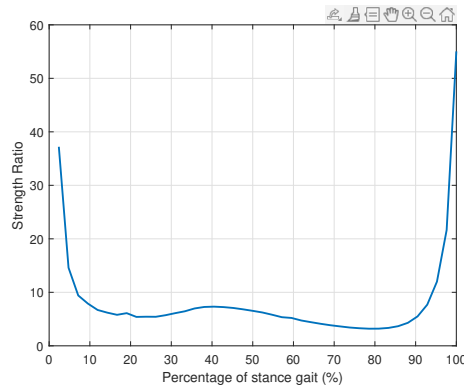


Figure 26: Evolution of strength ratio over time for one stance gait

Figure 27, demonstrates that in each case and for every criterion, the design is safe enough.

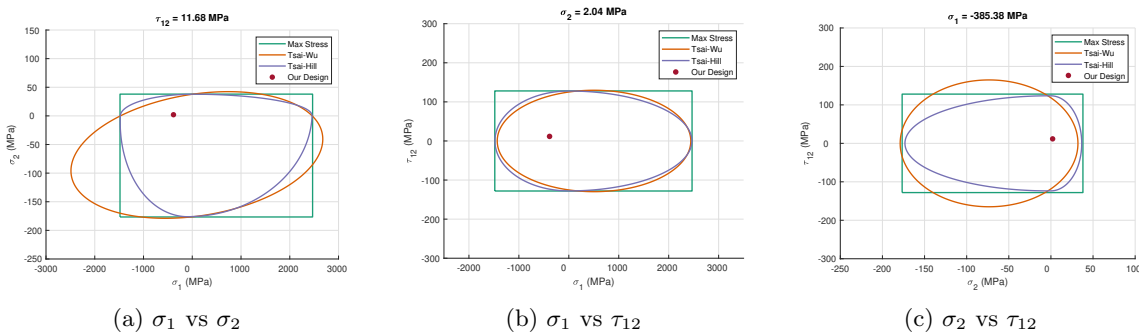


Figure 27: Failure loci for different failure criteria and our design

4.3.2 Weight-to-Strength Ratio Minimization

In this optimization, core thickness is also added to the optimization. This time, the weight-to-strength ratio is minimized for different numbers of layers. The choice of applying a sandwich structure is also added to the optimization to investigate its effect on the performance. The optimization options are also modified to find a global minimum in the optimization. This time, the number of layers between 36 to 46 is considered.

Please note that the genetic algorithm is a randomized method to find a minimum of the given function. Therefore, even though we manipulated the optimization parameters to calculate a global optimum, the results are subject to change in each run due to the random nature of the algorithm.

The following configuration is selected from the weight-strength ratio optimization. For 44 layers and a strength ratio of 3.54:

- **Upper kneel** using UD ply: $[0, 0, 0, 0, 0, 0, 0, 0, 0, -45, 90, 90, 45, 0, 0]_s$; a total of 30 layers
- **Lower kneel** using UD ply: $[0, 0, 0, 0, 0, 0, 0]_s$; a total of 14 layers

In Figure 28, the distributions of strain, stress, and strength ratio within the laminate are illustrated for the most critical timestep in the gait, identified as the heel-off phase.

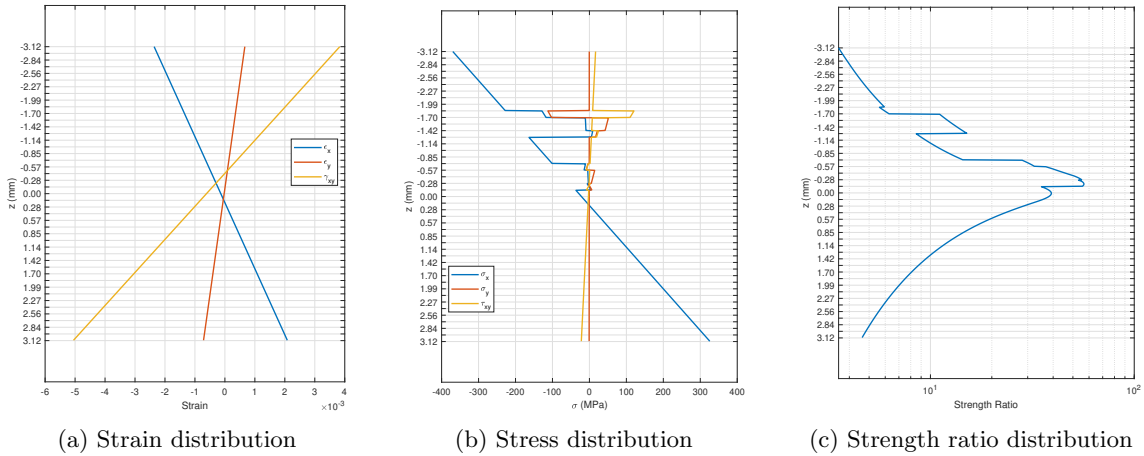


Figure 28: Strain, stress, and strength ratio distributions in the laminate for the most critical timestep.

Figure 29, shows the minimum strength ratio throughout the stance phase.

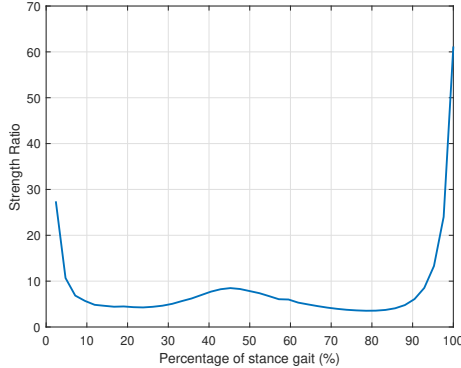


Figure 29: Evolution of strength ratio over time for one stance gait

Figure 30, demonstrates that in each case and for every criterion, the design is safe enough.

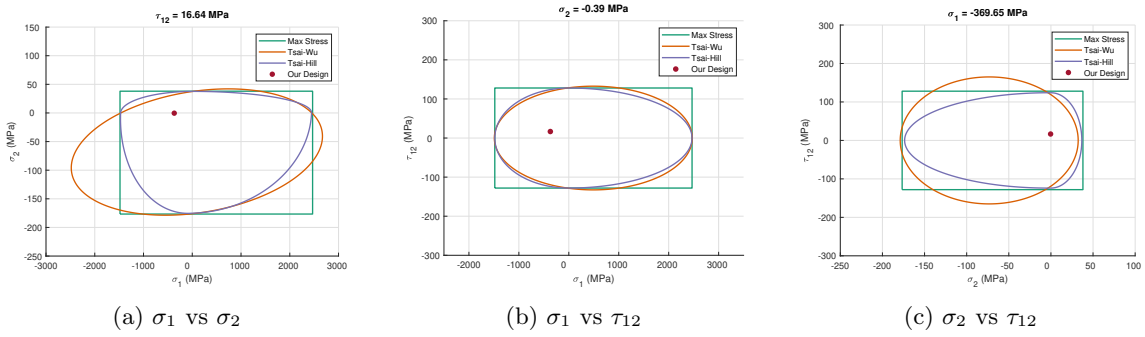


Figure 30: Failure loci for different failure criteria and our design

Please note that, in the optimization result, the core is not added by the optimization algorithm. In this case, a core can be added only due to cost considerations which we did not analyze in this study. Even though the SR of this design is larger, we found the design in the previous part more feasible due to the inclusion of layers oriented in different directions. As a rule of thumb, to have a feasible design, one must have at least 12.5% of laminates in other directions.

4.4 Selected Design

The following design is selected after the optimization:

- **Upper kneel** using UD ply: $[0, 0, 0, 0, 0, 0, 0, 0, 0, 0, -45, 90, 90, 45]_s$; a total of 30 layers
- **Lower kneel** using UD ply: $[0, 0, 0, 0, -45, 45, 0]_s$; a total of 14 layers

For this configuration mass and strength ratio values are found as:

- Total mass: 218.03 g
- Minimum strength ratio: 3.20

The found mass of the foot is reasonable. For most commercial products, the total weight of the design is between 500gr to 1000gr including the outer shell, which is about 250gr, depending on the user activity.

5 Conclusion

In this study, we aim to enhance the quality of life for patients with lower limb amputation by optimizing prosthetic feet, striving to reduce daily activity challenges, and narrowing the gap between an amputee and a healthy person. By strategically optimizing the orientation and arrangement of carbon fiber-reinforced polymer laminae, including both unidirectional and woven fabrics, and integrating a core material at the laminate center for cost-effectiveness and increased stiffness, we have aimed to strike a balance between enhanced functionality and practicality. Utilizing classical lamination theory and various failure theories for stress and strain calculations, our approach ensures a reliable design with an appropriate safety factor for patients of all weights. Finally, the validation of our optimized design using the finite element method reinforces the structural integrity and performance of the proposed configuration.

5.1 Future Work

One of the main shortcomings of this work is the thin-plate assumption. Stresses and strains perpendicular to the plate cannot be calculated with CLT. To improve this study, a FEM-based calculation can be implemented in MATLAB to obtain better optimization results. In addition, the energy storing aspect of the design is an important property to improve patient comfort. In this work, the energy-storing aspect of the foot is not calculated mathematically. Therefore, the strain energy of the design should be investigated throughout the gait and the optimum layer sequence must be calculated based on the result. Finally, most of the commercial products are machined to either connect upper and lower kneels with screws or to mitigate torsional effects at the foot center. Even though the best performance is achieved with UD fibers, the damage tolerance, and machinability of the design are also important for a prosthetic foot design. Therefore, woven fabrics can be implemented at the outer layers of the design or a different optimum sequence that combines two materials can be found in experiments.

5.2 Code Availability

Matlab code and additional visualizations can be accessed in our GitHub repository [21].

References

- [1] A. Steib and J.-P. Steib, "Pathologies osseuses dans l'Egypte ancienne," *Revue de Chirurgie Orthopédique et Traumatologique*, vol. 95, no. 5, pp. 477–483, 2009.
- [2] R. Versluys, A. Desomer, G. Lenaerts, *et al.*, "From conventional prosthetic feet to bionic feet: A review study," in *2008 2nd IEEE RAS & EMBS international conference on biomedical robotics and biomechatronics*, IEEE, 2008, pp. 49–54.
- [3] J. F. Lehmann, R. Price, S. Boswell-Bessette, A. Dralle, K. Questad, and B. J. deLateur, "Comprehensive analysis of energy storing prosthetic feet: Flex foot and seattle foot versus standard sach foot," *Archives of physical medicine and rehabilitation*, vol. 74, no. 11, pp. 1225–1231, 1993.
- [4] W. L. Childers and K. Z. Takahashi, "Increasing prosthetic foot energy return affects whole-body mechanics during walking on level ground and slopes," *Scientific reports*, vol. 8, no. 1, p. 5354, 2018.
- [5] A. E. Ferris, J. M. Aldridge, C. A. Rábago, and J. M. Wilken, "Evaluation of a powered ankle-foot prosthetic system during walking," *Archives of physical medicine and rehabilitation*, vol. 93, no. 11, pp. 1911–1918, 2012.
- [6] P. Cherelle, G. Mathijssen, Q. Wang, B. Vanderborght, and D. Lefeber, "Advances in propulsive bionic feet and their actuation principles," *Advances in mechanical engineering*, vol. 6, p. 984 046, 2014.
- [7] S. M. Jaegers, J. H. Arendzen, and H. J. de Jongh, "Prosthetic gait of unilateral transfemoral amputees: A kinematic study," *Archives of physical medicine and rehabilitation*, vol. 76, no. 8, pp. 736–743, 1995.
- [8] A. S. O. d. C. Soares, E. Y. Yamaguti, L. Mochizuki, A. C. Amadio, and J. C. Serrão, "Biomechanical parameters of gait among transtibial amputees: A review," *Sao Paulo Medical Journal*, vol. 127, pp. 302–309, 2009.
- [9] D. A. Winter, *Biomechanics and motor control of human movement*. John wiley & sons, 2009.
- [10] A. F. Şahin, M. F. Doğan, C. Uludoğan, *et al.*, *Microprocessor-Controlled-Prosthetic-Knee*, version 1.0.0, Jan. 2023. [Online]. Available: <https://github.com/mehmetfurkandogan/Microprocessor-Controlled-Prosthetic-Knee>.
- [11] O. Janeh and F. Steinicke, "A review of the potential of virtual walking techniques for gait rehabilitation," *Frontiers in Human Neuroscience*, vol. 15, p. 717291, 2021.
- [12] A. R. Tilley *et al.*, *The measure of man and woman: human factors in design*. John Wiley & Sons, 2001.
- [13] D. A. Berry, "Composite-materials for orthotics and prosthetics," *Orthotics and Prosthetics*, vol. 40, no. 4, pp. 35–43, 1987.
- [14] M. Rościszewska and M. Wekwejt, "Composites in energy storing prosthetic feet," *European Journal of Medical Technologies*, vol. 3, no. 20, pp. 16–22, 2018.
- [15] *Altair esacomp 4.7*. [Online]. Available: <https://altair.com/resource/altair-esacomp-datasheet>.
- [16] S. W. Tsai and E. M. Wu, "A general theory of strength for anisotropic materials," *Journal of composite materials*, vol. 5, no. 1, pp. 58–80, 1971.

- [17] S. W. Tsai and H. T. Hahn, “Introduction to composite materials, volume 1: Deformation of unidirectional and laminated composites,” Technical Report AFML-TR-78-201, Tech. Rep., 1978.
- [18] G. H. Staab, “5 - lamina failure theories,” in *Laminar Composites*, G. H. Staab, Ed., Woburn: Butterworth-Heinemann, 1999, pp. 142–190, ISBN: 978-0-7506-7124-8. DOI: <https://doi.org/10.1016/B978-075067124-8/50005-9>. [Online]. Available: <https://www.sciencedirect.com/science/article/pii/B9780750671248500059>.
- [19] M. Jiang and J. Zhang, “An investigation into the effect of cross-ply on energy storage and vibration characteristics of carbon fiber lattice sandwich structure bionic prosthetic foot,” *Science and Engineering of Composite Materials*, vol. 30, no. 1, 2023, ISSN: 21910359. DOI: 10.1515/secm-2022-0206.
- [20] A. D. Segal, K. E. Zelik, G. K. Klute, *et al.*, “The effects of a controlled energy storage and return prototype prosthetic foot on transtibial amputee ambulation,” *Human Movement Science*, vol. 31, no. 4, 2012, ISSN: 01679457. DOI: 10.1016/j.humov.2011.08.005.
- [21] M. F. Doğan, A. F. Şahin, W. Lasfar, and U. A. L. Closet, *Composite Laminate Optimization for Prosthetic Feet*, version 1.0.0, Jan. 2023. [Online]. Available: https://github.com/mehmetfurkandogan/composite_esar_foot.